Functional and molecular effects of TNF-α on human iPSC-derived cardiomyocytes

Anita Saraf[a,b,e,*], **Antonio Rampoldi**[b], **Myra Chao**[b], **Dong Li**[b], **Lawrence Armand**[b], **Hyun Hwang**[b], **Rui Liu**[b], **Rajnesh Jha**[b], **Haian Fu**[c], **Joshua T. Maxwell**[b], **Chunhui Xu**[b,d,*]

[a]Department of Medicine, Emory University School of Medicine, Atlanta, GA 30322, USA

[b]Department of Pediatrics, Emory University School of Medicine and Children's Healthcare of Atlanta, Atlanta, GA 30322, USA

[c]Emory Chemical Biology Discovery Center and the Department of Pharmacology and Chemical Biology, Emory University School of Medicine, Atlanta, GA 30322, USA

[d]Wallace H. Coulter Department of Biomedical Engineering, Georgia Institute of Technology and Emory University, Atlanta, GA 30322, USA

[e]University of Pittsburgh, Department of Medicine and Pediatrics and McGowan Regenerative Institute, 200 Lothorop Street, PUH, Pittsburgh, PA 15213, USA

Abstract

Proinflammatory molecule tumor necrosis factor alpha (TNF-α) is predominantly elevated in cytokine storm as well as worsening cardiac function. Here we model the molecular and functional effects of TNF-α in cardiomyocytes (CMs) derived from human induced pluripotent stem cells (hiPSC). We found that treatment of hiPSC-CMs with TNF-α increased reactive oxygen species (ROS) and caspase 3/7 activity and caused cell death and apoptosis. TNF-α treatment also resulted in dysregulation of cardiomyocyte function with respect to the increased abnormal calcium handling, calcium wave propagation between cells and excitation–contraction coupling. We also uncovered significant changes in gene expression and protein localization caused by TNF-α treatment. Notably, TNF-α treatment altered the expression of ion channels, dysregulated cadherins, and affected the localization of gap-junction protein connexin-43. In addition, TNF-α treatment up-regulated IL-32 (a human specific cytokine, not present in rodents and an inducer of TNF-α) and IL-34 and down-regulated glutamate receptors and cardiomyocyte contractile proteins. These findings provide insights into the molecular and functional consequences from the exposure of human cardiomyocytes to TNF-α. Our study provides a model to incorporate

*Corresponding authors at: University of Pittsburgh, 200 Lothorop Street, PUH, Pittsburgh, PA 15213 (A. Saraf). Emory University School of Medicine and Children's Healthcare of Atlanta, Atlanta, GA 30322, USA (C. Xu). saraf@pitt.edu (A. Saraf), chunhui.xu@emory.edu (C. Xu).

inflammatory factors into hiPSC-CM-based studies to evaluate mechanistic aspects of heart disease.

Keywords

Human iPSC; Cardiomyocytes; Cytokines; Ca^{2+} transients; TNFα; Ca^{2+}propagation

1. Introduction

Cytokines play a pivotal role in disease progression in cardiomyopathies and inflammatory diseases. Pro-inflammatory cytokine release associated with cardiomyopathies can affect matrix remodeling, oxidative stress and myocardial contraction and relaxation and trigger other inflammatory cells to mount additional immune responses within the myocardium (Heinrich et al., 2011; Aukrust et al., 1999; Dibbs et al., 1999; Matsumori, 1996; Matsumori et al., 1994; Mann, 2015; Schumacher and Naga Prasad, 2018).

Tumor necrosis factor alpha (TNF-α) is a key proinflammatory cytokine that is widely associated with worsening myocardial dysfunction and arrhythmias in diseases causing an increase in inflammatory milieu. The level of TNF-α is elevated in cardiomyopathy models and cardiac patients. For example, TNF-α levels are increased in the border zones of infarcted myocardium of rats with ligated coronary arteries (Chen et al., 2011) and in heart failure patients with New York Heart Association (NYHA) class II and III symptoms as compared with control subjects without heart failure and patients with NYHA Class I symptoms (Torre-Amione et al., 1996). Following myocardial infarction in a rat model, the arrhythmia burden increases in proportion to an increase in TNF-α (Chen et al., 2011). Similarly, post left anterior descending (LAD) ligation in rats, TNF-α reduces fractional shortening and the mean calcium transient amplitude (Feldman et al., 2000). More recently, TNF-α has been identified as a predominant cytokine in the cytokine storm associated with Coronavirus disease 2019 (COVID-19) related cardiomyopathies (Tisoncik et al., 2012; Wang et al., 2019; Feldmann et al., 2020).

TNF-α signaling has been elucidated in detail in primary cardiomyocytes (Bergmann et al., 2001; Jarrah et al., 2018; Al-Lamki et al., 2009; Condorelli et al., 2002) as well as in animal models of heart disease (Torre-Amione et al., 1996; Topkara et al., 2016; Evans et al., 2018; Matkovich et al., 2017). Results from human primary cardiomyocytes studies indicate that TNF-α increases the production of ROS and NF-κB thereby inducing apoptosis (Moe et al., 2014). Similarly, TNF-α also promotes depressed contractile activity in primary cardiomyocytes from multiple species (Cain et al., 1999). Studies from non-human cardiomyocytes have demonstrated altered calcium handling and decrease in connexin expression (Roe et al., 2015). However, to the best of our understanding, a comprehensive evaluation of the effect of TNF-α in *invitro* cardiomyocytes has not been performed. Therefore, in this study we performed a comprehensive analysis of TNF-α on hiPSC-CMs and potential molecular mechanisms associated with the functional changes.

2. Methods

2.1. hiPSC differentiation: Differentiation of hiPSCs into cardiomyocytes

SCVI 273 and IMR-90 hiPSCs were maintained in a feeder-free condition as described (Xu et al., 2001). IMR-90 hiPSC cells were induced sequentially with 100 ng/mL Activin A on differentiation day 0 and 10 ng/mL BMP4 on differentiation day 1 in RPMI containing 2% B27 without insulin (Preininger et al., 2016; Jha et al., 2016) for 96 h (Supplementary Fig. 1).

Similarly, SCVI 273 cells were expanded to 80–90% confluency and treated with 10 mM CHIR99021 HCl in RPMI with 2% B27 without insulin, to a final concentration of 6 μM for 48 h. Subsequently, cells were treated with 10 mM IWR to a final concentration of 10 μM for 48 h. Cell were then placed in RPMI containing 2% B27 with insulin until they started beating. Enriched cardiomyocytes were generated by assembling cardiospheres as previously described (Nguyen et al., 2014). Successful differentiation of hiPSCs was confirmed when beating was observed in majority of the cells in the culture. Furthermore, additional analyses including immunocytochemistry of NKX-2.5 and α-actinin were performed to examine differentiation efficiency using fluorescence microscopy and only those cultures where >85% of cells expressed cardiac markers of differentiation were used for further experiments. SCVI 273 were used for RNA-seq analysis. All other analyses were done with both SCVI 273 and IMR-90 cells.

2.2. DCFDA Assay

Cardiomyocytes were treated with 0.25% trypsin-EDTA and plated onto a Matrigel-coated 96-well culture plate at a density of 5×10^4 cells/well and cultured for 2 days to recover spontaneous beating. Treatment groups were maintained in TNF-α at predetermined concentrations. Cells were washed 2 times with warm D-PBS and incubated with 25 μM carboxy-H2DCFDA (ThermoFisher Scientific) working solution in warm HBSS/Ca^{2+}/Mg^{2+} for 30 min at 37 °C, protected from light. Cells were washed 3 times with warm HBSS/Ca^{2+}/Mg^{2+} and counter-stained with Hoechst in warm buffer and imaged immediately using Axio Vert.A1 inverted microscope (Zeiss).

2.3. Cell Viability

2D cultures as well as cardiac spheres were dissociated using 0.25% trypsin-EDTA and plated onto 96 well Matrigel-coated cell culture plates at the density of 5×10^4 cells/well and cultured for 2–3 days until they recovered beating. TNF-α at predetermined concentrations was added to the treatment groups and medium was changed every 24 h for 4 days. Cell viability was tested using 0.25 μM calcein-AM to label live cells and 1 μm ethidium homodimer-1 to label dead cells. Cells were incubated for 20 mins after which they were washed with D-PBS and resuspended in warm phenol red free RPMI.

2.4. Caspase 3/7 assay

Apoptosis was also assessed using Caspase 3/7 assay by adding CellEvent caspase 3/7 detection reagent to cells and incubating for 30 mins. Cells were subsequently washed with D-PBS and resuspended in warm phenol red free RPMI.

Cells were imaged using ArrayScan XTI Live high-content platform as described by Rampoldi et al (Rampoldi et al., 2018). Briefly, twenty fields/well and 5 replicate wells were selected per condition and imaged using a $10 \times$ objective. Cellomics Scan (ThermoFisher Scientific) was used for acquisition software to capture images, and data analysis was performed using Cellomics View Software (ThermoFisher Scientific). Images were analyzed with mask modifier for Hoechst restricted to the nucleus. Spot threshold was set to 10 units and detection limit was set to 25 units.

2.5. RNA-Seq analysis

RNA was isolated from 1.5×10^6 hiPSC-CMs per sample (n = 3/group) using Aurum total RNA mini kit (Bio-Rad) per manufacturer's instructions. Total RNA quality and purity were tested by agarose gel electrophoresis by Novogene Corporation Inc. The Illumina TruSeq technology was used to prepare RNA-Seq libraries, and next-generation sequencing was done via an Illumina HWI-ST1276. RNA sequence reads were aligned to the human reference genome using STAR v2.5. HTSeq v0.6.1 was used to count the read numbers mapped of each gene, and then Fragments per Kilobase of transcript sequence per Millions (FPKM) base pairs sequenced of each gene was calculated based on the length of the gene and reads count mapped to this gene to estimate gene abundance. Differential expression analysis was performed using the DESeq2 R package (2_1.6.3). The resulting p-values were adjusted using the Benjamini and Hochberg's approach for controlling the FDR. Genes were considered being up- or down-regulated when the adjusted p-value was < 0.05. GO enrichment analyses of DEGs were implemented by the cluster Profiler R package, in which gene length bias was corrected. DEGs with adjusted P-values<0.05 were used to identify the enriched GO terms and KEGG pathways.

2.6. Fluo-4 AM loading

For live cell imaging of intracellular Ca^{2+}, the cells were incubated with 10 μM of Fluo-4 AM (ThermoFisher Scientific) for 20 min at 37 °C in culture medium, washed for 10 min, and then transferred to an inverted laser confocal microscope (Olympus FV1000) equipped with FluoView software (Olympus), where they were perfused with normal tyrode solution (140 mM NaCl, 4 mM KCl, 2 mM $CaCl_2$, 1 mM $MgCl_2$, 10 mM HEPES, 5 mM glucose, pH 7.4 with NaOH) (Lian *et al.*, 2012). Fluo-4 was excited by the 488 nm laser and emitted fluorescence was captured at > 505 nm. Recordings of Fluo-4 fluorescence were acquired in line-scan mode along the longitudinal axis at a sampling rate of 500 lines per second and a pixel size of 0.155 μm. Regions exhibiting heterogeneous fluorescence of Fluo-4 were avoided, so as to exclude artifacts (e.g, endoplasmic reticulum, mitochondria, vesicles, etc.). Data were analyzed with ClampFit 10.0 software (Molecular Devices). As differentials in Fluo-4 loading efficiency between cell lines can influence observed fluorescence intensities, loading and acquisition conditions were kept as consistent as possible, and all absolute fluorescence (F) measurements were normalized to inherent basal (i.e. background) fluorescence (F_0). Estimates of intracellular Ca2 + are presented as changes in F/F_0, where F = F – F_0.

2.7. Ca^{2+} sparks analysis

Quantification of Ca^{2+} sparks was performed on line-scans using the SparkMaster plugin (Picht et al., 2007) for ImageJ (NIH). Regions for analysis were selected from the portions outside the action potential-induced transient. Fluorescence amplitudes were measured, normalized to basal fluorescence, and expressed as   F/F$_0$. As recommended by the SparkMaster algorithm developers (Picht et al., 2007), a detection criteria threshold of 3.8 was selected in which the detection of events was 3.8 times the standard deviation of the background noise divided by the mean. Representative output images were generated using the 'F/F$_0$′ setting available in the plugin.

2.8   Single cell Ca^{2+} transient assay:

Differentiated cardiomyocytes were seeded in 96-well plates 20×104 cells/well. Cells were allowed to recover beating for 1–3 days after which they were incubated with 5 μM Fluo-4 AM for 15 min at 37°C. Cells were then washed with 1X Normal Tyrode solution (148 mM NaCl, 4 mM KCl, 0.3 mM NaPH2O4·H2O, 5 mM HEPES, 0.5 mM MgCl2·6H2O, 10 mM D-Glucose, 1.8 mM CaCl2·H2O, pH adjusted to 7.4 with NaOH). Change in calcium fluorescence was recorded by acquiring images immediately using the ImageXpress Micro XLS System (Molecular Devices) (Ex: 488 nm Em:515–600 nm, Frequency: 5 frames/s, 20x magnif ication for 12 s totally). Regions of interest within the cytoplasm were selected and fluorescence intensities were measured over time for individual cells using MetaXpress. Normal versus abnormal readout of Ca^{2+} transients were determined using previously published methods (Rampoldi et al., 2019).

2.8. Ca^{2+} propogation across cardiomyocytes

Differentiation batches with high cardiomyocyte purity (>90%) were selected for this assay. Cells were seeded at 50×10^4 cells/well in a 96 well clear bottom plate. Cells were allowed to recover beating at for 1–3 days after which they were incubated with 5 μM Fluo-4 as noted above. Images were acquired as noted above using ImageXpress Micro XLS System (Molecular Devices). 30 s videos were recorded and processed using Image J. A transverse imaginary line was drawn across the screen and 6–8 cell on either side of the line were selected simultaneously. Fluorescence intensity graphed over time simultaneously. Fluorescence patterns that were most frequent were considered to be dominant and hence in synchrony with each other. Abnormal patterns as well as lack of change in fluorescence were considered to be abnormal.

2.9. Contractility

Contractility of hiPSC-CMs was recorded using a phase contrast inverted microscope (Axio Vert.A1) equipped with Zeiss AxioCam digital camera system, at 40 × magnification with recordings of 30 s for each sample at 100 ms interval between frames. Videos were processed and exported using Zeiss AxioVision LE imaging software. Video-based analysis of contractility parameters was performed with Matlab R2016b software as previously described (Huebsch et al., 2015).

2.10.   Immunohistochemistry

Adherent cells were rinsed with cold PBS and fixed with 2% para-formaldehyde solution for 15 min at room temperature, permeabilized with ice-cold 100% methanol for 2 min, rinsed again with 1x PBS, and blocked for 1 hr with 5% normal goat serum (NGS; Thermo Fisher). Cells were incubated overnight with primary antibodies, then rinsed three times with $1 \times$ PBS to remove excess antibody. Cells were incubated with fluorescently conjugated secondary antibodies for 1 h at RT in the dark. Cells were then washed three more times with $1 \times$ PBS. Nuclear counterstaining was performed using Hoecht. Cells were imaged with a phase contrast and fluorescence AxioVert A1 inverted microscope (Zeiss) equipped with AxioCam digital camera system (Zeiss). Images were exported using AxioVision LE (Zeiss) and merging was performed in Adobe Photoshop.

3.   Results

3.1.   TNF-α increases cytoplasmic ROS production and cell death in hiPSC-CMs

We generated enriched hiPSC-CMs (Supplemental Fig. 1) and treated them for 4 days with TNF-α at concentrations ranging from 1 to 100 ng/mL - TNF-α has physiologic effects on cardiomyocytes at 1 ng/mL and pathologic effects on cardiomyocytes at 20 and 100 ng/mL (Shanmugam et al., 2016). During the TNF-α treatment, we measured cytoplasmic ROS activity daily with DCFDA. There was an increase in the level of ROS in the TNF-α treated cells at day 2 (Fig. 1a and 1b). At day 3 and day 4, the level of ROS was higher in the cells treated with 20 and 100 ng/mL compared with the cells treated with 1 and 10 ng/mL (Fig. 1a and 1b). We also assessed caspase activity and cell viability. Caspase 3/7 activity increased from day 2 to day 4 after the TNF-α treatment with maximal activity noted with 20 and 100 ng/mL at day 3 and 4. (Fig. 1c and 1d). In addition, increased number of dead cells (positive by ethidium iodide staining) was detected at day 4 cells treated with 20 and 100 ng/mL of TNF-α (Fig. 2).

3.2.   TNF-α upregulates pathways related to autophagy and chronic cellular stress and activates pathways of innate immunity

To gain molecular insight into the effect of TNF-α treatment, we conducted RNA-Seq analysis after the treatment of hiPSC-CMs with 20 ng/mL TNF-α for 4 days. In this treatment condition, while there was only a small decrease in the viability of cells (see Figs. 1 and 2), a significant portion of cells showed robust functional dysregulation (see the following sections). From the RNA-Seq analysis, we identified 6565 genes that were differentially expressed in hiPSC-CMs treated with TNF-α versus untreated controls (Fig. 3a). Of these, 3115 genes were upregulated and 3450 genes were downregulated. We note that TNF-α upregulated *TNFR1* and dysregulated multiple downstream proteins that are associated with its receptors TNFR1 and TNFR2 (Supplemental Fig. 1).

Using Gene Ontology (GO) enrichment analysis, we found that 819 significant terms were differentially regulated ($p < 0.05$), among which the most significantly affected "biological process", "cellular component" and "molecular function" are shown in Fig. 3b. Genes in upregulated biological pathways were associated with autophagy (adj p-value = 2.36×10^{-14}), organelle stress (adj p-value 4.1×10^{-10}), protein ubiquitination (adj p-value =

2.89×10^{-8}) indicating increased degradation of cellular proteins, and other catabolic processes including the activation of NF-kB pathway (adj p-value = 1.06×10^{-4}). Pathways activating the innate immune response were also upregulated. Specifically, cytokines such as IL-32 (5.98 log2 fold, adj p-value 2.23×10^{-281}) and IL-34 (3.96 log2 fold, adj p-value 2.00×10^{-26}) involved in the activation of chronic inflammatory responses involving T-cells were among the top 10 upregulated by the fold change (number 1 and 3 respectively).

We note that, in the GO enrichment analysis, individual differentially expressed genes could be involved in multiple functional and mechanistic pathways (Fig. 3c). For example, genes associated with calcium handling such as *CACNB2* and *CAMK2A* were involved with cardiac muscle contraction, arrhythmia, necroptosis, adrenergic signaling, TGF-β signaling, NF-κB signaling in addition to calcium handling, suggesting that TNF-α affects multiple pathways associated with normal cardiomyocyte function.

3.3. TNF-α downregulates genes involved in cytoskeletal architecture, calcium ion signaling and energy regulation

GO enrichment analysis identified downregulation of genes involved in cardiomyocyte architecture (Fig. 3), including those associated with myofibril assembly (adj p-value = 1.63×10^{-13}) and included cellular components involved with myocardial contraction (adj p value = 2.9×10^{-17}) such as sarcomeres (adj p-value = 1.39×10^{-6}): I band (adj p-value = 1.23×10^{-11}), Z disc (adj p-value = 4.44×10^{-11}), A band (adj p-value = 1.08×10^{-6}) and actomyosin complex (adj p-value = 1.47×10^{-12}). Calcium handling pathways were also downregulated including genes involved with intracellular calcium stores such as sarcoplasmic reticulum (adj p-value = 1.72×10^{-16}) and T-tubules (adj p-value = 6.8×10^{-4}) and calcium ion signaling (adj p-value = 3.36×10^{-7}). In addition, multiple pathways associated with oxidation–reduction (adj p-value = 7.6×10^{-4}), NADH activity (adj p-value = 4.2×10^{-4}) as well as cellular aerobic respiration (adj p-value = 5.83×10^{-8}) were also downregulated. These data suggest that TNF-α causes extensive cytoskeletal remodeling as well as downregulation of functional proteins involved in energy regulation, aerobic respiration and calcium handling.

3.4. TNF-α induces abnormal calcium handling in hiPSC-CMs and increases arrhythmogenic events

To examine if calcium handling was affected in hiPSC-CMs treated with TNF-α, we conducted Ca^{2+} imaging analysis to exam global intracellular calcium transients with cytosolic Ca^{2+} indicator Fluo-4AM. Cytosolic Ca^{2+} transients showed a dose-dependent increase in abnormal waveforms from 28% in untreated cells to 83% in cells treated with 100 ng/mL TNF-α (Fig. 4a). The number of complex arrhythmias as noted in Fig. 4b increased as concentration of TNF-α increased from 1 ng/mL to 100 ng/mL. We also examined the incidence of calcium sparks in TNF-α treated hiPSC-CMs. Ca^{2+} sparks are elementary Ca^{2+} release events from the SR in the heart that represent a major pathway for the leak of Ca^{2+} and pose as a potential substrate for the activation of arrhythmogenic Ca^{2+} waves. Fig. 4c shows examples of confocal line-scan images and corresponding local Fluo-4 fluorescence profiles (F/F_0) of Ca^{2+} sparks from untreated and TNF-α treated hiPSC-CMs. A significant increase in the Ca^{2+} spark frequency was observed in cells treated with   10

ng/mL TNF-α (Fig. 4d). Similarly, spark amplitude was significantly increased in cells treated with   10 ng/mL TNF-α (Fig. 4d). The proportion of cells that showed propagating Ca^{2+} waves during spark recordings increased with increased concentrations of TNF-α (Fig. 5d).

3.5.   TNF-α regulates the expression of multiple ion channels in hiPSC-CMs

With RNA-Seq analysis, we also manually identified differentially expressed genes that encode ion channels and Ca^{2+} handling proteins because of their involvement in cardiac function (Fig. 4e). Among the down-regulated genes were *SERCA* channel *ATP2A2* (0.62 log2 fold, padj = 6.28×10^{-20}) and *ATP2A3* (0.415 log2 fold downregulation, padj = 1.44×10^{-06}), sodium calcium exchanger *SLC8A1* (0.54 log2 fold, padj = 8.21×10^{-10}) and *SLC8A-AS1* (0.44 log2 fold, padj = 2.34×10^{-05}), and ryanodine receptor *RYR2* (0.69 log2 fold, padj = 4.57×10^{-19}) and *RYR3* (1.06 log2 fold, padj = 1.85×10^{-5}). *SERCA* channels regulate the sarcoplasmic reticulum (SR) calcium store and thus the amount of calcium available for release with each action potential; the sodium calcium exchangers are involved in removing calcium from the cytosol after systole, thereby promoting the relaxation of cardiomyocytes, and ryanodine receptors regulates the release of Ca^{2+} from sarcoplasmic reticulum to the cytosol. Among the up-regulated genes was Inositol 1,4,5-trisphosphate receptor *ITPR1* (0.61 log2 fold, padj = 1.29×10^{-3}). In addition, several potassium ion channels and glutamate inotropic receptors were also up- and down-regulated (Fig. 4e).

3.6.   TNF-α dose-dependently disrupts intercellular calcium propagation

We further examined if hiPSC-CMs treated with TNF-α showed abnormality in calcium propagation across a sheet of cardiomyocytes. Using fluorescence imaging to monitor changes in intracellular calcium concentration in a field of hiPSC-CMs, we recorded multiple neighboring cells from a sheet of beating cardiomyocytes after exposing them to increasing concentrations of TNF-α (Fig. 5a). We determined the proportion of cells within cardiomyocyte sheets (n = 11–7) that were beating synchronously or asynchronously with respect to each other. In the untreated culture, 87% of the cardiomyocytes displayed synchronous beating across cell sheets (Fig. 6b). In the culture untreated with 1 ng/mL TNF-α, the majority of the cells (72%) showed synchronous beating and 28% of the cells showed asynchronous beating (Fig. 5b and 5c). The percentage of asynchrony further increased in cultures treated with 10 and 20 ng/mL TNF-α (52% and 56% respectively). At 100 ng/mL TNF-α, a significant portion of cells did not beat or were asynchronous with neighboring cells (65%). Videos of Ca^{+2} propagation in with different concentrations of TNF-α are available in Video Supplemental S1, S2, S3, S4, S5.

Given these observations, we investigated changes of gap junction and adherent proteins because of their involvement in coordinated action potential propagation. At the RNA level, we found from our RNA-Seq dataset that gap junction protein *GJA5* (connexin 40), *GJB1* (connexin 32), *GJB2* (connexin 26) and *GJD2* (connexin 36) were significantly down-regulated (Fig. 6d). We also found that numerous proteins from the cadherin family were up- or downregulated in TNF-α treated samples (Fig. 6a). Cadherins are cell adhesion molecules responsible for maintaining mechanical and electrical coupling between cardiomyocytes. At the protein level, we conducted confocal immunohistochemistry analyses with antibodies

against pan-cadherin and connexin 43. We observed decreased localization of these proteins to the plasma membrane with increasing concentrations of TNF-α (Fig. 6b); note that fluorescence signals were observed in plasma membrane in cells treated with 1 ng/mL TNF-α but was also localized intracellularly in cells treated with 20 and 100 ng/mL TNF-α.

These observations indicate that TNF-α decreased inter-cellular calcium propagation, dysregulated the expression of cell–cell adhesion proteins and gap junction proteins, and affected the localization of connexin-43 and cadherin.

3.7. TNF-α decreases cardiomyocyte contractility

Given the observed abnormal Ca^{2+} transients and dyssynchronous Ca^{2+} propagation, we next compared cardiac contractility between untreated and TNF-α treated hiPSC-CMs using a video-based method (Huebsch et al., 2015). The beat rate as well as contraction and relaxation velocity decreased significantly with increasing concentrations of TNF-α from 1 ng/mL to 100 ng/mL (Fig. 7a). Additionally, irregular beats were noted with increasing frequency with higher concentrations of TNF-α (Fig. 7b). These results further prompted us to examine the relative expression of genes involved in cardiomyocyte contraction. In the RNA-Seq dataset, we observed a downregulation of multiple proteins associated with mechanoenergetics including ATPAses and cytochrome C; calcium gated channels, as well as contractile proteins associated with myosin, tropomyosin, troponin and actin (Fig. 7c).

4. Discussion

TNF-α is a pleiotropic cytokine that has both beneficial and harmful effects based on the signaling pathways it activates. In most cell types, pathological doses of TNF-α induces the caspase signaling pathway that promotes ROS production, catabolic protein processing, autophagy and cell death (Al-Lamki et al., 2009; Condorelli et al., 2002; Cain et al., 1999). In human primary cardiomyocytes, TNF-α increases the production of ROS and induces NF-κB activation (Roe et al., 2015). In non-human cardiomyocytes, TNF-α reduces connexin expression and alters calcium handling (Heinrich et al., 2011; George et al., 2017; Liew et al., 2013). Similarly, in our hiPSC-CM model, TNF-α increased caspase activity and NF-κB signaling, induced ROS production and altered the expression of ion channels, connexins and cadherins, which could have contributed dysregulation of functional and molecular pathways, such as abnormal Ca^{2+} transient and contractility TNF-α treatment caused a dose-dependent increase in Ca^{2+} sparks and waves that led to abnormal Ca^{2+} transients and increased arrhythmogenic patterns of conductance. Molecularly, TNF-α treatment altered the expression of ion channels, downregulated cadherins, and affected the localization of gap-junction protein connexin-43. In addition, TNF-α treatment up-regulated IL-32 (a human specific cytokine) and IL-34 and down-regulated glutamate receptors and cardiomyocyte contractile proteins. These results provide novel insights into the complex functional and molecular aspects of TNF-α signaling in human cardiomyocytes. This study also provides a proof-of-concept that disease specific inflammatory factors should be incorporated into hiPSC-CM-based studies to evaluate mechanistic aspects of heart disease as these inflammatory factors can modulate cell behavior.

Our study with hiPSC-CMs not only complement findings in non-human cells and animal models but also provides novel insights into the TNF-α signaling in humans and identifications novel cellular factors not seen in rodents. Rodent cardiomyocytes differ significantly in their electrical and mechanical properties from human cardiomyocytes as rodent hearts beat at a much faster rate of 300–600 beats per minute, thereby creating inherent limitations in the understanding of normal and diseased cardiovascular physiology (Anzai et al., 2020; Mummery, 2018). For example, repolarization currents driven by K + as well as the composition of myosin within rodent versus human cardiomyocytes are different (Mummery, 2018; Giacomelli et al., 2017; Rajamohan et al., 2013). Human cardiomyocytes also express unique cytokines that are absent in the rodents. Indeed, we found that IL-32, a proinflammatory cytokine that is found only in higher mammals but not in rodents (Xuan et al., 2017) was upregulated with the highest fold change after the TNF-α treatment. IL-32 was reported to be significantly elevated in patients with heart failure (HF) and related to the severity of HF (Xuan et al., 2017). IL-32 itself is an inducer of TNF-α (Kim et al., 2005), suggesting a tight link between these molecules in hiPSC-CMs. Another cytokine, IL-34 was also upregulated with the third highest fold change after TNF-α exposure. Increased serum IL-34 levels were reported to be associated with cardiac dysfunction in patients with ischemic cardiomyopathy (Xi et al., 2018).

Treatment of hiPSC-CMs with TNF-α induced the up-regulation of TNF-α receptor *TNFR1* but it did not affect the expression of *TNFR2*. This observation is consistent with the role of these receptors in the heart-––studies have shown that TNF-α interaction with TNFR1 leads to increase in inflammatory response and cardiotoxicity, whereas the TNF-α-TNFR2 interaction has a protective effect (Al-Lamki et al., 2009; Defer et al., 2007). Similar to published models of TNF-α signaling (Al-Lamki et al., 2009; Evans et al., 2018; Chang et al., 2006; Haudek et al., 2007) multiple downstream transcription factors (Fos, Jun, JunB), matrix metalloproteinases (MMP14, MMP25), and factors associated with leukocyte recruitment and activation (CCL2, CXCL1, CXCL2, CXCL3, CSF1) were also upregulated in hiPSC-CMs treated with TNF-α.

Functionally, TNF-α treatment caused a dose dependent increase in calcium sparks and waves in hiPSC-CMs that lead to abnormal calcium transients. hiPSC-CMs also mounted an increase in ROS in response to TNF-α treatment, which has been implicated in literature to cause abnormal calcium handling and arrhythmogenic events. Furthermore, TNF-α treatment caused a disruption of intercellular pathways that increased arrhythmogenic patterns of conductance across cardiomyocytes, which likely resulted from downregulation of cadherins as well as changes in the localization of gap-junction protein connexin-43.

Clinically, heart failure is associated not only with the loss of myocardial contractile forces due to disrupted mechanoenergetics, but also with an increased susceptibility to arrhythmias due to dysregulation of ion channels that are integral to optimal cardiomyocyte function. Heart failure affects multiple calcium handling channels through decreased expression of SERCA (SR Ca^{2+} ATPase), increased leakiness of RyR2 and changing NCX function and expression that together affect the cytosolic concentration of Ca^{2+} (Roe et al., 2015; Gomez et al., 1997; Heinzel et al., 2008). Our study revealed a similar transcriptomic profile in hiPSC-CMs treated with TNF-α (*e.g.*, decreased SERCA and NCX expression).

In addition to dysregulated calcium transients within cells, our study demonstrates that hiPSC-CM sheets can model disrupted calcium propagation with increasing concentration of TNF-α. Cadherins as well as connexins 43, 40 and 45 (which are expressed in different subsets of cardiomyocytes) contribute to organization of gap junctions that dictate patterns of current flow, synchronizing the global heart rhythm (Severs et al., 2004a, 2004b, 2006c; Wong et al., 2017; Lillo et al., 2019; Mahtab et al., 2012). We found that TNF-α treatment downregulated cadherin and gap junction proteins and altered the localization of connexin-43 in hiPSC-CMs, thereby increasing asynchronous and non-conducting cells. In the intact heart, asynchronous cells can serve as foci of arrhythmogenesis, and non-functional cells can be a barrier to normal electrical conduction pathways. Therefore, our findings suggest the increased susceptibility of the heart to arrhythmias in a pro-inflammatory milieu.

Our study also demonstrates a dose-dependent decrease in beat rate, contraction and relaxation velocity in hiPSC-CMs treated with TNF-α. Hearts inflicted with cardiomyopathies have a prolonged repolarization duration due to downregulation of various potassium channels. Cardiomyocytes of animals and patients with heart failure show a prolonged action potential duration, indicative of a decrease in potassium channels that bring about repolarization (Rahm et al., 2018) (Severino et al., 2020). Our transcriptomics analysis revealed a similar dysregulation of potassium channels in hiPSC-CMs treated with TNF-α. We found that a few potassium channels were upregulated but the majority of potassium channels are downregulated. Proteins associated with Ito (Kv 4.2, Kv 4.3), the predominant potassium channel modified in heart failure (Niwa and Nerbonne, 2010), were not found to be differentially expression in hiPSC-CMs treated with TNF-α. However, within the heart, Ito has regional differences in expression patterns with a decreased overall expression in the endocardium as compared to the epicardium (Niwa and Nerbonne, 2010).

Systolic and diastolic disruption is a hallmark of various cardiomyopathies as well as other conditions such as sepsis where TNF-α concentration is increased (Goldhaber et al., 1996; Kelly and Smith, 1997). This has mechanistically been associated with alterations in sarcoplasmic architecture as well as calcium handling proteins (Goldhaber et al., 1996), which was demonstrated in our study. Additionally, our transcriptomics analysis also revealed a downregulation of various contractile proteins as well as calcium gated channels in hiPSC-CMs treated with TNF-α, similar to those seen in animal models (Goldhaber et al., 1996; Kelly and Smith, 1997; Janczewski et al., 2003)

Lastly, transcriptomics analysis showed a significant dysregulation of glutamate receptors in hiPSC-CMs (Fig. 6d). While glutamate receptors are found to be abundant in the brain, they are not predominantly expressed in hearts of non-human mammals. Therefore, the role of glutamate receptors in the human heart is poorly understood. However, multiple glutamate receptors have been identified within excitatory cells of the atrial and ventricular cardiomyocytes and have been implicated in altering calcium handling with cells (Tchervenkov et al., 2000). Therefore, a translational hiPSC-CM model can help elucidate the role of glutamate receptors in cardiomyopathies and other diseases with a pro-inflammatory milieu. In summary, despite the relative immaturity nature of the hiPSC-CMs used in our study, multiple functional and molecular alteration can be induced by the

treatment of TNF-α. This human cardiomyocyte model can be further exploited to mimic physiologic conditions associated with cardiomyopathy and inflammation.

5. Limitations

Our study provides a comprehensive analysis of molecular and functional responses of pro-inflammatory molecule TNF-α in hiPSC-CMs as an in vitro translation model. hiPSC-CMs are unique in that they are culture adapted to maintain viability for weeks, whereas primary cardiomyocytes survive in vitro for only a few days, thereby limiting their translatability of external stimuli from in vivo models. However, hiPSC-CMs studied here are considered to be immature, in that their contractile proteins, gene expression profile, the number of calcium ion channels and calcium handling genes, as well as mitochondrial and SR density resemble those of the fetal cardiomyocytes. Consequently, while our study shows that hiPSC-CMs can replicate pathways activated by TNF-α, similar to those activated in primary cardiomyocytes and in in vivo studies, there may be inherent limitations to those responses due to the fetal nature of hiPSC-CMs.

6. Conclusions

In summary, despite the relative immaturity nature of the hiPSC-CMs used in our study, multiple functional and molecular alterations can be induced by the treatment of TNF-α. This human cardiomyocyte model can be further exploited to mimic physiologic conditions associated with cardiomyopathy and inflammation. Cardiomyocytes derived from hiPSCs can faithfully model numerous aspects of viability, intracellular molecular signaling, calcium handling and contraction profiles in response to TNF-α. Furthermore, using human derived cells elucidated the role of novel biomarkers such as IL-32 and IL-34 as well as glutamate receptors that are not dominant in other animal models.

7. Data availability statement

Supplementary Material

Refer to Web version on PubMed Central for supplementary material.

References

Heinrich M, Oberbach A, Schlichting N, Stolzenburg JU, Neuhaus J, 2011. Cytokine effects on gap junction communication and connexin expression in human bladder smooth muscle cells and suburothelial myofibroblasts. PloS one 6.

Aukrust P, Ueland T, Lien E, Bendtzen K, Muller F, Andreassen AK, Nordoy I, Aass H, Espevik T, Simonsen S, Froland SS, Gullestad L, 1999. Cytokine network in congestive heart failure secondary to ischemic or idiopathic dilated cardiomyopathy. The American journal of cardiology 83, 376–382. [PubMed: 10072227]

Dibbs Z, Kurrelmeyer K, Kalra D, Seta Y, Wang F, Bozkurt B, Baumgarten G, Sivasubramanian N, Mann DL, 1999. Cytokines in heart failure: pathogenetic mechanisms and potential treatment. Proc Assoc Am Physicians 111, 423–428. [PubMed: 10519163]

Matsumori A, 1996. Cytokines in myocarditis and cardiomyopathies. Curr Opin Cardiol 11, 302–309. [PubMed: 8835873]

Matsumori A, Yamada T, Suzuki H, Matoba Y, Sasayama S, 1994. Increased circulating cytokines in patients with myocarditis and cardiomyopathy. Br Heart J 72, 561–566. [PubMed: 7857740]

Mann DL, 2015. Innate immunity and the failing heart: the cytokine hypothesis revisited. Circ Res 116, 1254–1268. [PubMed: 25814686]

Schumacher SM, Naga Prasad SV, 2018. Tumor Necrosis Factor-alpha in Heart Failure: an Updated Review. Curr Cardiol Rep 20, 117. [PubMed: 30259192]

Chen Y, Zhang Q, Liao YH, Cao Z, Du YM, Xia JD, Yang H, Chen ZJ, 2011. Effect of tumor necrosis factor-alpha on neutralization of ventricular fibrillation in rats with acute myocardial infarction. Mediators Inflamm 2011, 565238. [PubMed: 21584281]

Torre-Amione G, Kapadia S, Lee J, Durand JB, Bies RD, Young JB, Mann DL, 1996. Tumor necrosis factor-alpha and tumor necrosis factor receptors in the failing human heart. Circulation 93, 704–711. [PubMed: 8640999]

Feldman AM, Combes A, Wagner D, Kadakomi T, Kubota T, Li YY, McTiernan C, 2000. The role of tumor necrosis factor in the pathophysiology of heart failure. Journal of the American College of Cardiology 35, 537–544. [PubMed: 10716453]

Tisoncik JR, Korth MJ, Simmons CP, Farrar J, Martin TR, Katze MG, 2012. Into the eye of the cytokine storm. Microbiol Mol Biol Rev 76 (1), 16–32. [PubMed: 22390970]

Wang L, He W, Yu X, Hu D, Bao M, Liu H, Zhou J, Jiang H, Coronavirus disease, 2019. in elderly patients: Characteristics and prognostic factors based on 4-week follow-up. J Infect 80 (2020), 639–645.

Feldmann Marc, Maini Ravinder N, Woody James N, Holgate Stephen T, Winter Gregory, Rowland Matthew, Richards Duncan, Hussell Tracy, 2020. Trials of anti-tumour necrosis factor therapy for COVID-19 are urgently needed. Lancet 395 (10234), 1407–1409. [PubMed: 32278362]

Bergmann MW, Loser P, Dietz R, von Harsdorf R, 2001. Effect of NF-kappa B Inhibition on TNF-alpha-induced apoptosis and downstream pathways in cardiomyocytes. Journal of molecular and cellular cardiology 33, 1223–1232. [PubMed: 11444925]

Jarrah Andrew A., Schwarskopf Martina, Wang Edward R., LaRocca Thomas, Dhume Ashwini, Zhang Shihong, Hadri Lahouria, Hajjar Roger J., Schecter Alison D., Tarzami Sima T., 2018. SDF-1 induces TNF-mediated apoptosis in cardiac myocytes. Apoptosis 23 (1), 79–91. [PubMed: 29236198]

Al-Lamki RS, Brookes AP, Wang J, Reid MJ, Parameshwar J, Goddard MJ, Tellides G, Wan T, Min W, Pober JS, Bradley JR, 2009. TNF receptors differentially signal and are differentially expressed and regulated in the human heart. Am J Transplant 9, 2679–2696. [PubMed: 19788501]

Condorelli G, Morisco C, Latronico MV, Claudio PP, Dent P, Tsichlis P, Condorelli G, Frati G, Drusco A, Croce CM, Napoli C, 2002. TNF-alpha signal transduction in rat neonatal cardiac myocytes: definition of pathways generating from the TNF-alpha receptor. FASEB J 16, 1732–1737. [PubMed: 12409315]

Topkara VK, Chambers KT, Yang KC, Tzeng HP, Evans S, Weinheimer C, Kovacs A, Robbins J, Barger P, Mann DL, 2016. Functional significance of the discordance between transcriptional profile and left ventricular structure/function during reverse remodeling. JCI Insight 1.

Evans S, Tzeng HP, Veis DJ, Matkovich S, Weinheimer C, Kovacs A, Barger PM, Mann DL, 2018. TNF receptor-activated factor 2 mediates cardiac protection through noncanonical NF-kappaB signaling. JCI Insight 3.

Matkovich Scot J., Al Khiami Belal, Efimov Igor R., Evans Sarah, Vader Justin, Jain Ashwin, Brownstein Bernard H., Hotchkiss Richard S., Mann Douglas L., 2017. Widespread Down-Regulation of Cardiac Mitochondrial and Sarcomeric Genes in Patients With Sepsis. Crit Care Med 45 (3), 407–414. [PubMed: 28067713]

Moe KT, Khairunnisa K, Yin NO, Chin-Dusting J, Wong P, Wong MC, 2014. Tumor necrosis factor-alpha-induced nuclear factor-kappaB activation in human cardiomyocytes is mediated by NADPH oxidase. J Physiol Biochem 70, 769–779. [PubMed: 25059721]

Cain Brian S., Meldrum Daniel R., Dinarello Charles A., Meng Xianzhong, Joo Kyung S., Banerjee Anirban, Harken Alden H., 1999. Tumor necrosis factor-alpha and interleukin-1beta synergistically depress human myocardial function. Crit Care Med 27 (7), 1309–1318. [PubMed: 10446825]

Roe AT, Frisk M, Louch WE, 2015. Targeting cardiomyocyte Ca2+ homeostasis in heart failure. Curr Pharm Des 21, 431–448. [PubMed: 25483944]

Xu Chunhui, Inokuma Margaret S., Denham Jerrod, Golds Kathaleen, Kundu Pratima, Gold Joseph D., Carpenter Melissa K., 2001. Feeder-free growth of undifferentiated human embryonic stem cells. Nat Biotechnol 19 (10), 971–974. [PubMed: 11581665]

Preininger Marcela K., Jha Rajneesh, Maxwell Joshua T., Wu Qingling, Singh Monalisa, Wang Bo, Dalal Aarti, Mceachin Zachary T., Rossoll Wilfried, Hales Chadwick M., Fischbach Peter S., Wagner Mary B., Xu Chunhui, 2016. A human pluripotent stem cell model of catecholaminergic polymorphic ventricular tachycardia recapitulates patient-specific drug responses. Disease Models & Mechanisms 9 (9), 927–939. [PubMed: 27491078]

Jha R, Wu Q, Singh M, Preininger MK, Han P, Ding G, Cho HC, Jo H, Maher KO, Wagner MB, Xu C, 2016. Simulated Microgravity and 3D Culture Enhance Induction. Viability, Proliferation and Differentiation of Cardiac Progenitors from Human Pluripotent Stem Cells, Scientific Reports 6, 30956. [PubMed: 27492371]

Nguyen DC, Hookway TA, Wu Q, Jha R, Preininger MK, Chen X, Easley CA, Spearman P, Deshpande SR, Maher K, Wagner MB, McDevitt TC, Xu C, 2014. Microscale generation of cardiospheres promotes robust enrichment of cardiomyocytes derived from human pluripotent stem cells. Stem Cell Reports 3, 260–268. [PubMed: 25254340]

Rampoldi Antonio, Crooke Stephen N., Preininger Marcela K., Jha Rajneesh, Maxwell Joshua, Ding Lingmei, Spearman Paul, Finn MG, Xu Chunhui, 2018. Targeted Elimination of Tumorigenic Human Pluripotent Stem Cells Using Suicide-Inducing Virus-like Particles. ACS Chemical Biology 13 (8), 2329–2338. [PubMed: 29979576]

Picht Eckard, Zima Aleksey V., Blatter Lothar A., Bers Donald M., 2007. SparkMaster: automated calcium spark analysis with ImageJ. Am J Physiol Cell Physiol 293 (3), C1073–C1081. [PubMed: 17376815]

Rampoldi A, Singh M, Wu Q, Duan M, Jha R, Maxwell JT, Bradner JM, Zhang X, Saraf A, Miller GW, Gibson G, Brown LA, Xu C, 2019. Cardiac Toxicity From Ethanol Exposure in Human-Induced Pluripotent Stem Cell-Derived Cardiomyocytes. Toxicol Sci 169, 280–292. [PubMed: 31059573]

Huebsch Nathaniel, Loskill Peter, Mandegar Mohammad A., Marks Natalie C., Sheehan Alice S., Ma Zhen, Mathur Anurag, Nguyen Trieu N., Yoo Jennie C., Judge Luke M., Spencer C. Ian, Chukka Anand C., Russell Caitlin R., So Po-Lin, Conklin Bruce R., Healy Kevin E., 2015. Automated Video-Based Analysis of Contractility and Calcium Flux in Human-Induced Pluripotent Stem Cell-Derived Cardiomyocytes Cultured over Different Spatial Scales. Tissue Eng Part C Methods 21 (5), 467–479. [PubMed: 25333967]

Shanmugam G, Narasimhan M, Sakthivel R, Kumar RR, Davidson C, Palaniappan S, Claycomb WW, Hoidal JR, Darley-Usmar VM, Rajasekaran NS, 2016. A biphasic effect of TNF-alpha in regulation of the Keap1/Nrf2 pathway in cardiomyocytes. Redox Biol 9, 77–89. [PubMed: 27423013]

George SA, Calhoun PJ, Gourdie RG, Smyth JW, Poelzing S, 2017. TNFalpha Modulates Cardiac Conduction by Altering Electrical Coupling between Myocytes. Front Physiol 8, 334. [PubMed: 28588504]

Liew R, Khairunnisa K, Gu Y, Tee N, Yin NO, Naylynn TM, Moe KT, 2013. Role of tumor necrosis factor-alpha in the pathogenesis of atrial fibrosis and development of an arrhythmogenic substrate. Circ J 77, 1171–1179. [PubMed: 23370453]

Anzai T, Yamagata T, Uosaki H, 2020. Comparative Transcriptome Landscape of Mouse and Human Hearts. Front Cell Dev Biol 8, 268. [PubMed: 32391358]

Mummery Christine L., 2018. Perspectives on the Use of Human Induced Pluripotent Stem Cell-Derived Cardiomyocytes in Biomedical Research. Stem Cell Reports 11 (6), 1306–1311. [PubMed: 30540958]

Giacomelli E, Mummery CL, Bellin M, 2017. Human heart disease: lessons from human pluripotent stem cell-derived cardiomyocytes. Cellular and molecular life sciences : CMLS 74 (20), 3711–3739. [PubMed: 28573431]

Rajamohan Divya, Matsa Elena, Kalra Spandan, Crutchley James, Patel Asha, George Vinoj, Denning Chris, 2013. Current status of drug screening and disease modelling in human pluripotent stem cells. Bioessays 35 (3), 281–298. [PubMed: 22886688]

Xuan Wanling, Huang Weixing, Wang Ruijie, Chen Chang, Chen Yequn, Wang Yan, Tan Xuerui, 2017. Elevated circulating IL-32 presents a poor prognostic outcome in patients with heart failure after myocardial infarction. Int. J. Cardiol 243, 367–373. [PubMed: 28747035]

Kim SH, Han SY, Azam T, Yoon DY, Dinarello CA, 2005. Interleukin-32: a cytokine and inducer of TNFalpha. Immunity 22, 131–142. [PubMed: 15664165]

Xi R, Fan Q, Yan X, Zhang H, Xie H, Gu G, Xu Y, Wang F, Tao R, 2018. Increased Serum Interleukin-34 Levels Are Related to the Presence and Severity of Cardiac Dysfunction in Patients With Ischemic Cardiomyopathy. Frontiers in physiology 9, 904. [PubMed: 30050466]

Defer N, Azroyan A, Pecker F, Pavoine C, 2007. TNFR1 and TNFR2 signaling interplay in cardiac myocytes. J Biol Chem 282, 35564–35573. [PubMed: 17913704]

Chang L, Kamata H, Solinas G, Luo JL, Maeda S, Venuprasad K, Liu YC, Karin M, 2006. The E3 ubiquitin ligase itch couples JNK activation to TNFalpha-induced cell death by inducing c-FLIP(L) turnover. Cell 124, 601–613. [PubMed: 16469705]

Haudek SB, Taffet GE, Schneider MD, Mann DL, 2007. TNF provokes cardiomyocyte apoptosis and cardiac remodeling through activation of multiple cell death pathways. J Clin Invest 117, 2692–2701. [PubMed: 17694177]

Gomez AM, Valdivia HH, Cheng H, Lederer MR, Santana LF, Cannell MB, McCune SA, Altschuld RA, Lederer WJ, 1997. Defective excitation-contraction coupling in experimental cardiac hypertrophy and heart failure. Science 276, 800–806. [PubMed: 9115206]

Heinzel FR, Bito V, Biesmans L, Wu M, Detre E, von Wegner F, Claus P, Dymarkowski S, Maes F, Bogaert J, Rademakers F, D'Hooge J, Sipido K, 2008. Remodeling of T-tubules and reduced synchrony of Ca2+ release in myocytes from chronically ischemic myocardium. Circ Res 102, 338–346. [PubMed: 18079411]

Severs NJ, Coppen SR, Dupont E, Yeh HI, Ko YS, Matsushita T, 2004. Gap junction alterations in human cardiac disease. Cardiovasc Res 62, 368–377. [PubMed: 15094356]

Severs NJ, Dupont E, Coppen SR, Halliday D, Inett E, Baylis D, Rothery S, 2004. Remodelling of gap junctions and connexin expression in heart disease. Biochim Biophys Acta 1662, 138–148. [PubMed: 15033584]

Severs NJ, Dupont E, Thomas N, Kaba R, Rothery S, Jain R, Sharpey K, Fry CH, 2006. Alterations in cardiac connexin expression in cardiomyopathies. Adv Cardiol 42, 228–242. [PubMed: 16646594]

Wong P, Laxton V, Srivastava S, Chan YW, Tse G, 2017. The role of gap junctions in inflammatory and neoplastic disorders (Review). Int J Mol Med 39, 498–506. [PubMed: 28098880]

Lillo MA, Himelman E, Shirokova N, Xie LH, Fraidenraich D, Contreras JE, 2019. S-nitrosylation of connexin43 hemichannels elicits cardiac stress-induced arrhythmias in Duchenne muscular dystrophy mice. JCI Insight 4.

Mahtab EA, Gittenberger-de Groot AC, Vicente-Steijn R, Lie-Venema H, Rijlaarsdam ME, Hazekamp MG, Bartelings MM, 2012. Disturbed myocardial connexin 43 and N-cadherin expressions in

hypoplastic left heart syndrome and borderline left ventricle. The Journal of thoracic and cardiovascular surgery 144, 1315–1322. [PubMed: 22405962]

Rahm AK, Lugenbiel P, Schweizer PA, Katus HA, Thomas D, 2018. Role of ion channels in heart failure and channelopathies. Biophys Rev 10, 1097–1106. [PubMed: 30019205]

Severino P, D'Amato A, Pucci M, Infusino F, Birtolo LI, Mariani MV, Lavalle C, Maestrini V, Mancone M, Fedele F, 2020. Ischemic Heart Disease and Heart Failure: Role of Coronary Ion Channels. Int J Mol Sci 21.

Niwa N, Nerbonne JM, 2010. Molecular determinants of cardiac transient outward potassium current (I(to)) expression and regulation. Journal of molecular and cellular cardiology 48, 12–25. [PubMed: 19619557]

Goldhaber JI, Kim KH, Natterson PD, Lawrence T, Yang P, Weiss JN, 1996. Effects of TNF-alpha on [Ca2+]i and contractility in isolated adult rabbit ventricular myocytes. Am J Physiol 271 (4), H1449–H1455. [PubMed: 8897939]

Kelly RA, Smith TW, 1997. Cytokines and cardiac contractile function. Circulation 95, 778–781. [PubMed: 9054727]

Janczewski AM, Kadokami T, Lemster B, Frye CS, McTiernan CF, Feldman AM, 2003. Morphological and functional changes in cardiac myocytes isolated from mice overexpressing TNF-alpha, American journal of physiology. Heart and circulatory physiology 284, H960–969. [PubMed: 12578819]

Tchervenkov Christo I, Jacobs Marshall L, Tahta Stephen A, 2000. Congenital Heart Surgery Nomenclature and Database Project: hypoplastic left heart syndrome. Ann Thorac Surg 69 (3), 170–179.
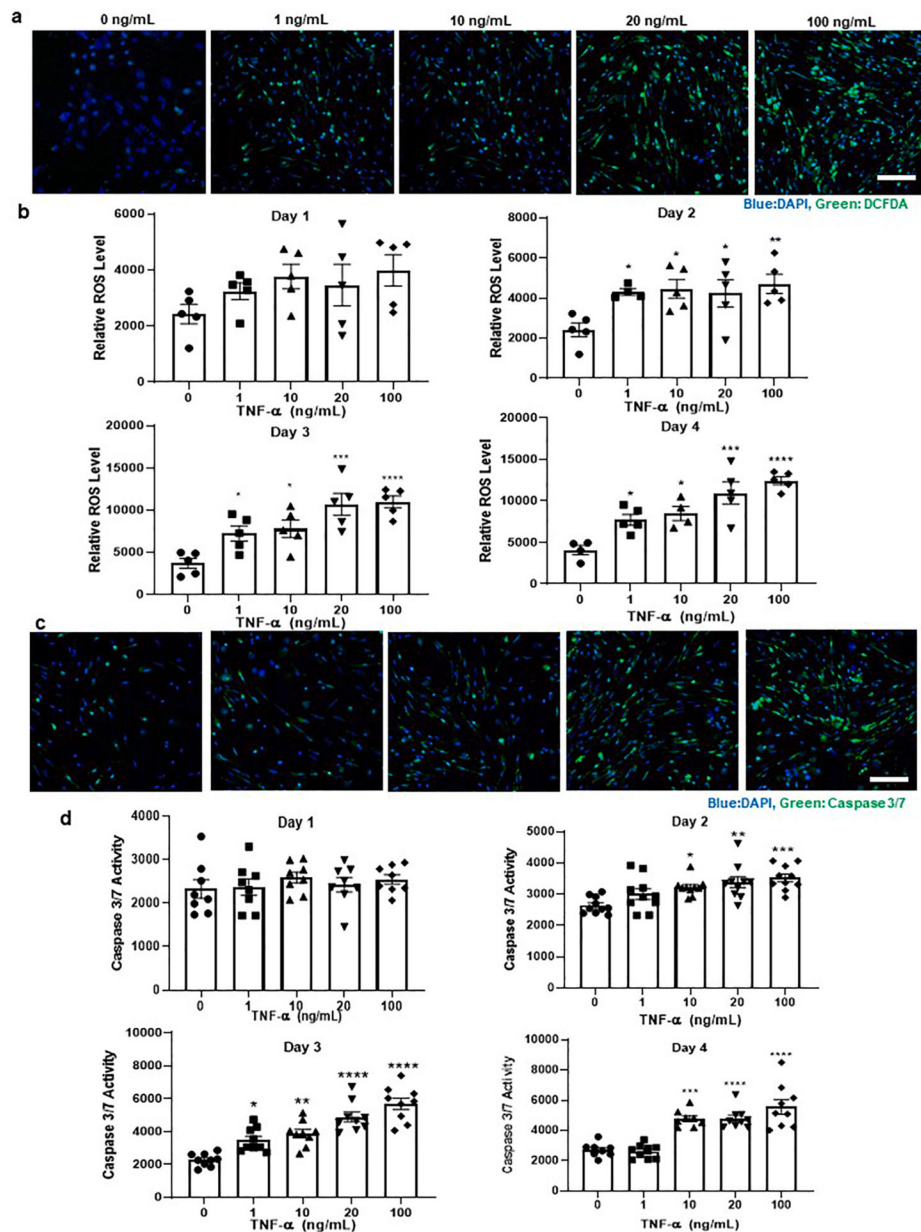
Fig. 1.
TNF-α induced a dose-dependent increase of cytoplasmic reactive oxygen species (ROS) and apoptosis in hiPSC-CMs (a) Representative images using SCVI 273 showing the detection of cellular ROS detected with DCFDA dye (green). (b) As compared with the control group, cytoplasmic ROS level increased from day 2 with increasing doses of TNF-α. The relative ROS level is presented as mean fluorescence intensity of DCFDA ± standard error of the mean (SEM) (n = 4–5). Statistical analyses were performed by one-way ANOVA and post-hoc analysis was performed by Dunnett's multiple comparison test. (c) Apoptosis of cardiomyocytes after TNF-α treatment was tested using caspase 3/7 assay (green). (d) Caspase 3/7 activity in cultures treated with various doses of TNF-α over 4 days. The relative caspase 3/7 activity is presented as mean fluorescence intensity of caspase 3/7 signal

± standard error of the mean (SEM). Statistical analyses were performed by one-way ANOVA. (n = 9–10). *p < 0.05, **p < 0.01, *** p < 0.001, ****p < 0.0001. Bar represents 100 μm.
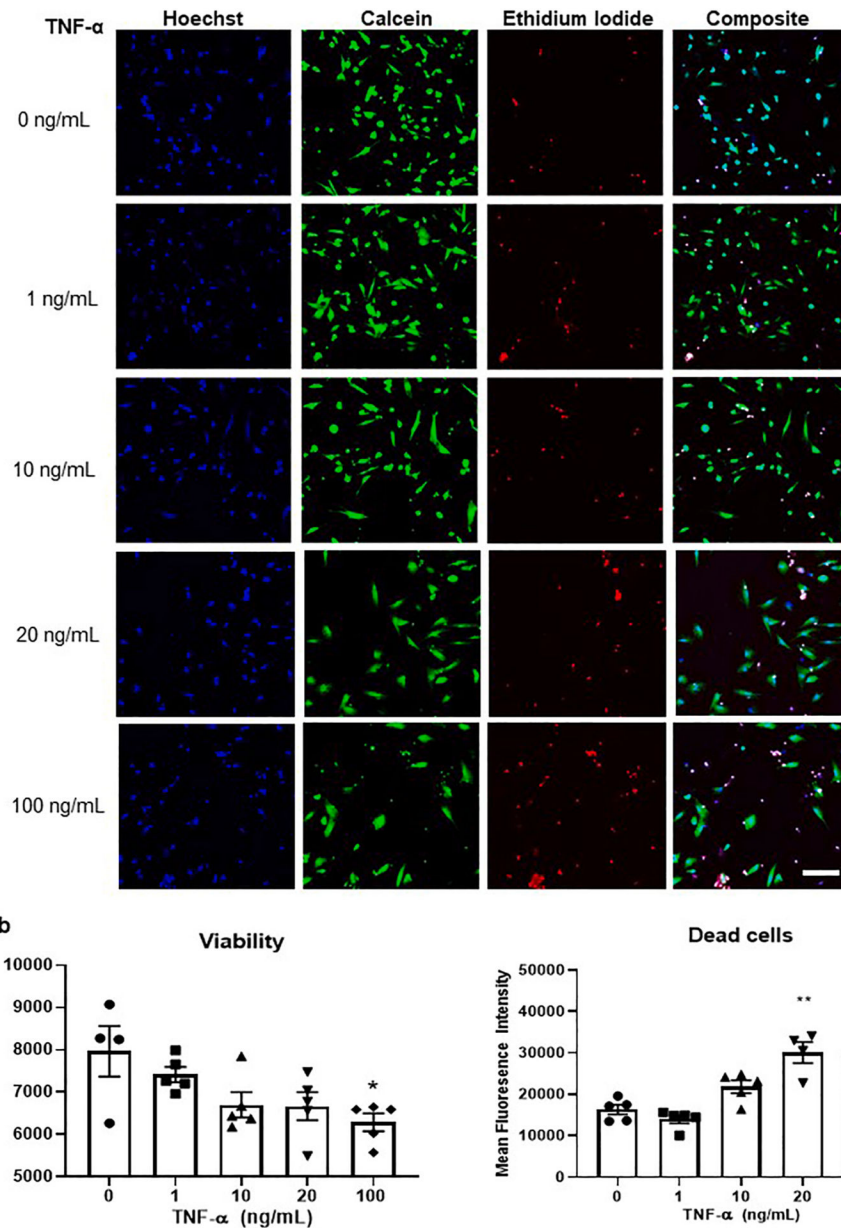
Fig. 2.

TNF-α caused a dose-dependent increase in cell death and decrease in cell viability in hiPSC-CMs. (a) Representative images from CMs derived from iPSC cell line SCVI 273. Cell death was measured using Live/dead cell viability assay after 4 days of TNF-α treatment. Live cells were detected with calcein (green) dye and dead cells were detected using ethidium-homodimer (red) using high throughput Arrayscan. (b) The effect of doses of TNF-α on cell viability and apoptosis represent mean value ± standard error of the mean (SEM), and statistical analyses were performed by one-way ANOVA and post-hoc analysis was performed by Dunnett's multipole comparison test (n = 4–6). *p < 0.05, **p < 0.01, *** p < 0.001, ****p < 0.0001. Bar represents 20 μm.
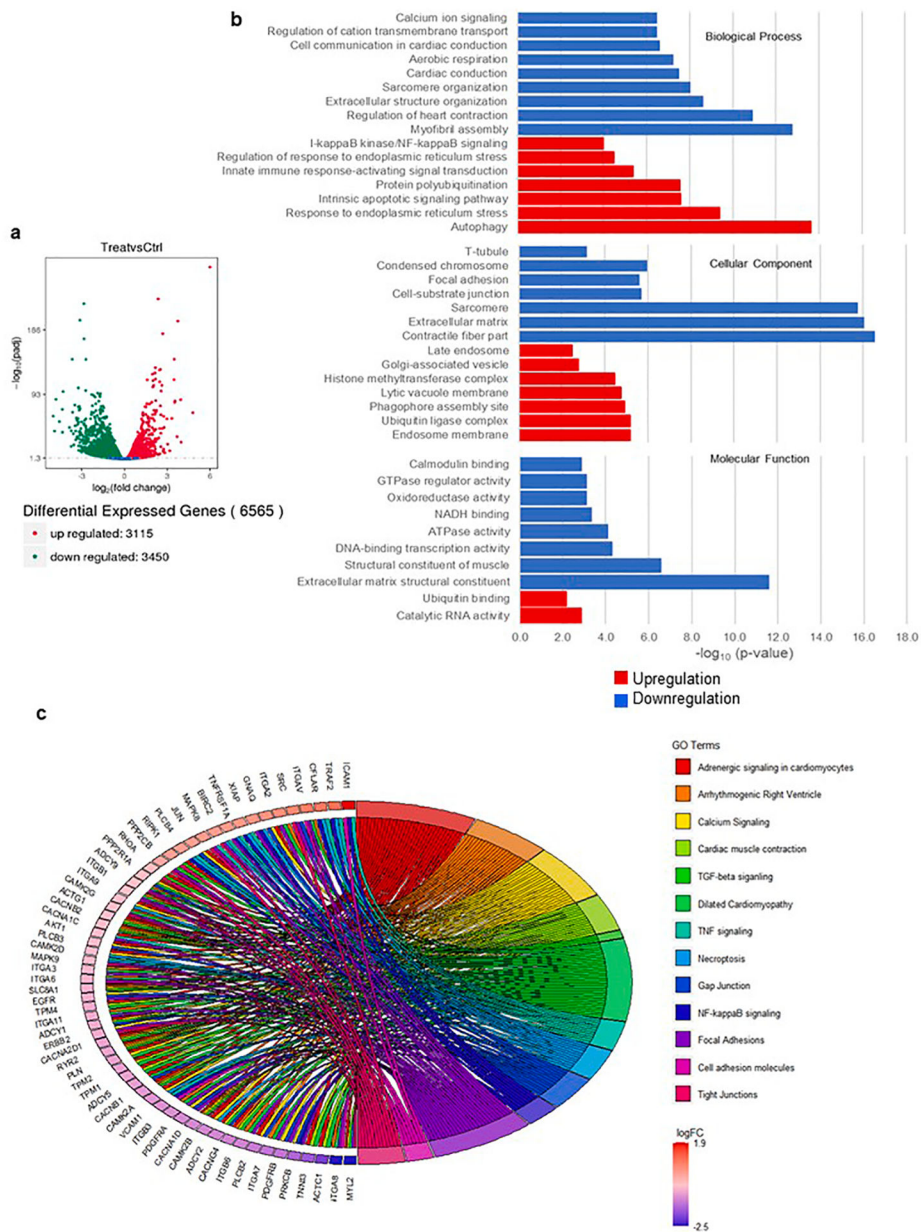
Fig. 3.
Differentially expressed genes and gene ontology (GO) terms dysregulated by the treatment with 20 ng/mL TNF-α. (a) Volcano plot of differentially expressed genes. (b) GO terms represented as bar plots of upregulated (red) and downregulated (blue) genes where the length of the bar directly correlates to gene enrichment score on a −log10(p-value) scale. (c) Chord diagram showing relationship between GO clusters associated with functional properties of cardiomyocytes (right, legend) and corresponding genes contributing to these enrichment (left).
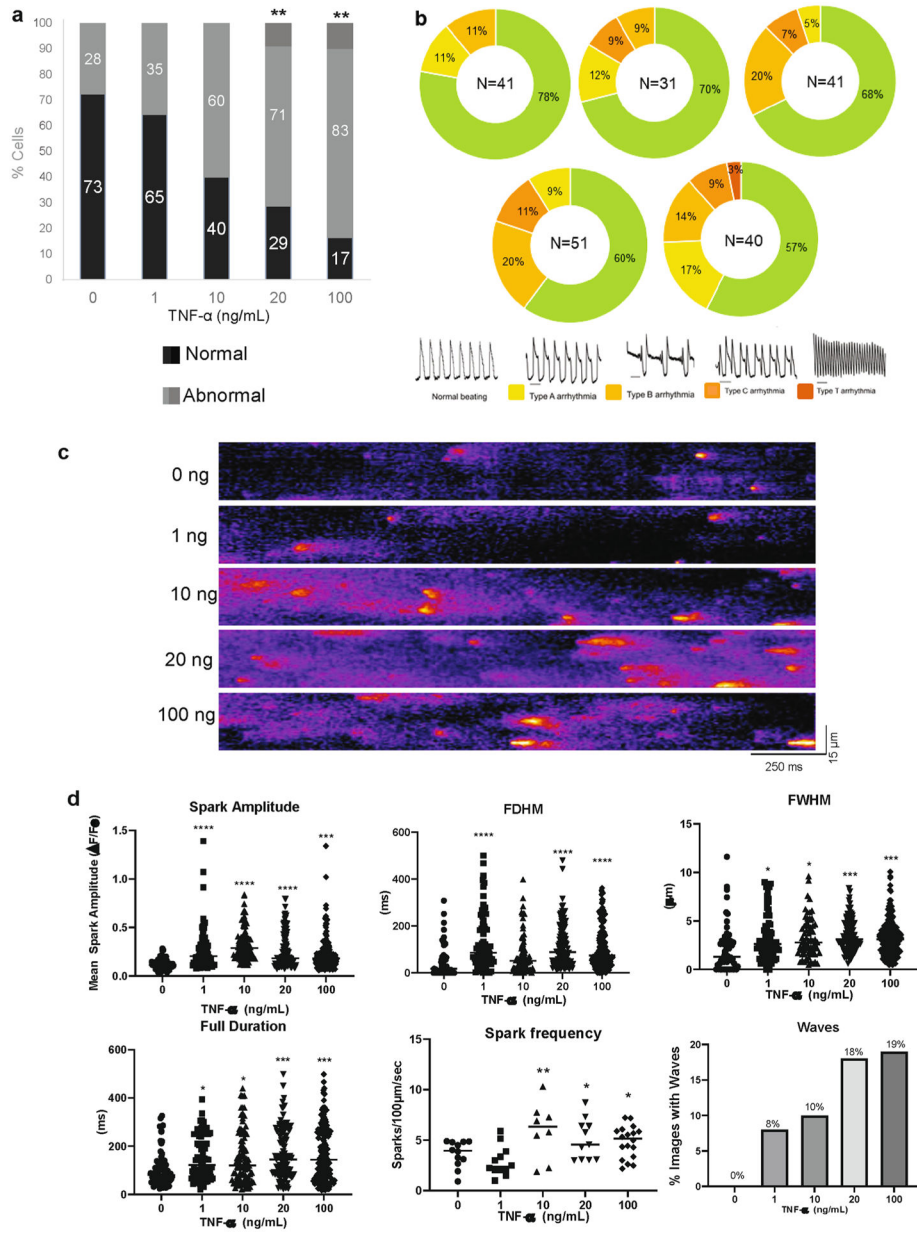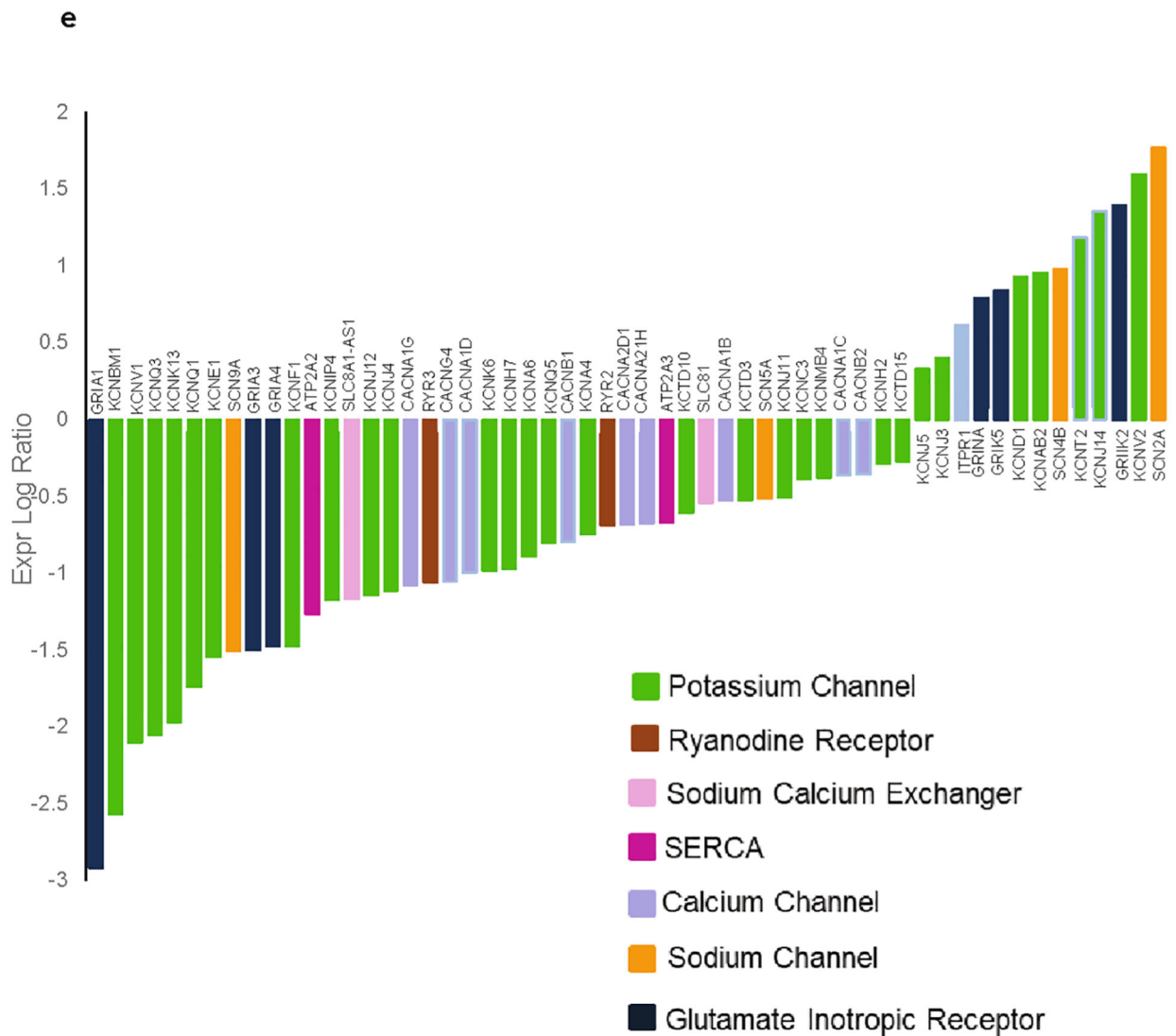
Fig. 4.
TNF-α caused a dose-dependent increase in abnormal calcium transients (a) Proportion of cardiomyocytes with normal or abnormal intracellular Ca^{2+} transients after treatment with TNF-α. Statistical analysis was performed two-way ANOVA with post-hoc analysis with Chi-square $*p < 0.05$, $**p < 0.01$. (b) Pie charts showing the percentage of cells with normal or abnormal subtypes of Ca^{2+} transients. (c) Representative confocal images of cytosolic Ca^{+2} traces showing sparks and waves. (d) Summary of spark amplitude, full width, half maximum (FWHM) amplitude, full duration, half magnitude (FDHM) and full duration of spontaneous Ca^{+2} sparks under various TNF-α concentrations. Sample sizes (*n*) are denoted in the center of the graphs for the control and treatment groups. (e) Transcriptomics analysis of upregulation and downregulation of ion channels after treatment with 20 ng/mL TNF-α. Bar graph denotes expression log ratios of upregulation in the positive Y axis and downregulation in the negative Y axis. Ion channels are color coded as noted in the legend.
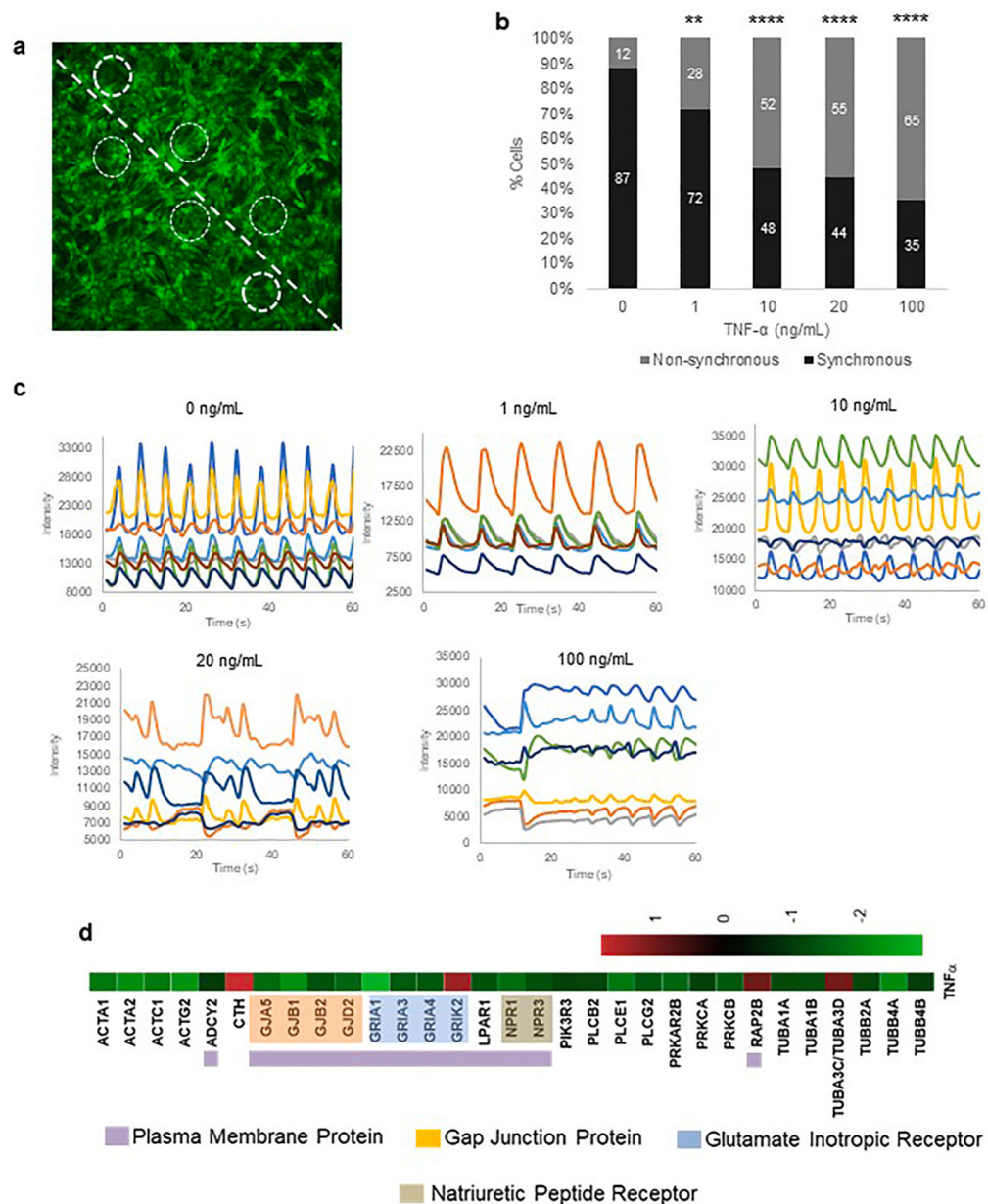
Fig. 5.
Propagation of Ca^{2+} across a sheet of cardiomyocytes. (a) Representative Ca^{+2} images where 6 regions were chosen (circled) across the sheet of CMs derived from SCVI 273 and IMR 90, at equidistant points and the intracellular Ca^{+2} traces were recorded with respect to each other. (b) Stacked bar graphs showing dose response to TNF-α as a proportion of synchronous and asynchronous cells. Statistical analysis was performed two-way ANOVA with post-hoc analysis with Chi-square. **$p < 0.01$, ****$p < 0.0001$ (c) Representative waveforms of hiPSC-CMs treated with increasing concentrations of TNF-α. (d) Transcriptomics analysis of plasma membrane proteins demonstrating that multiple gap junction proteins are downregulated when exposed to TNF-α.
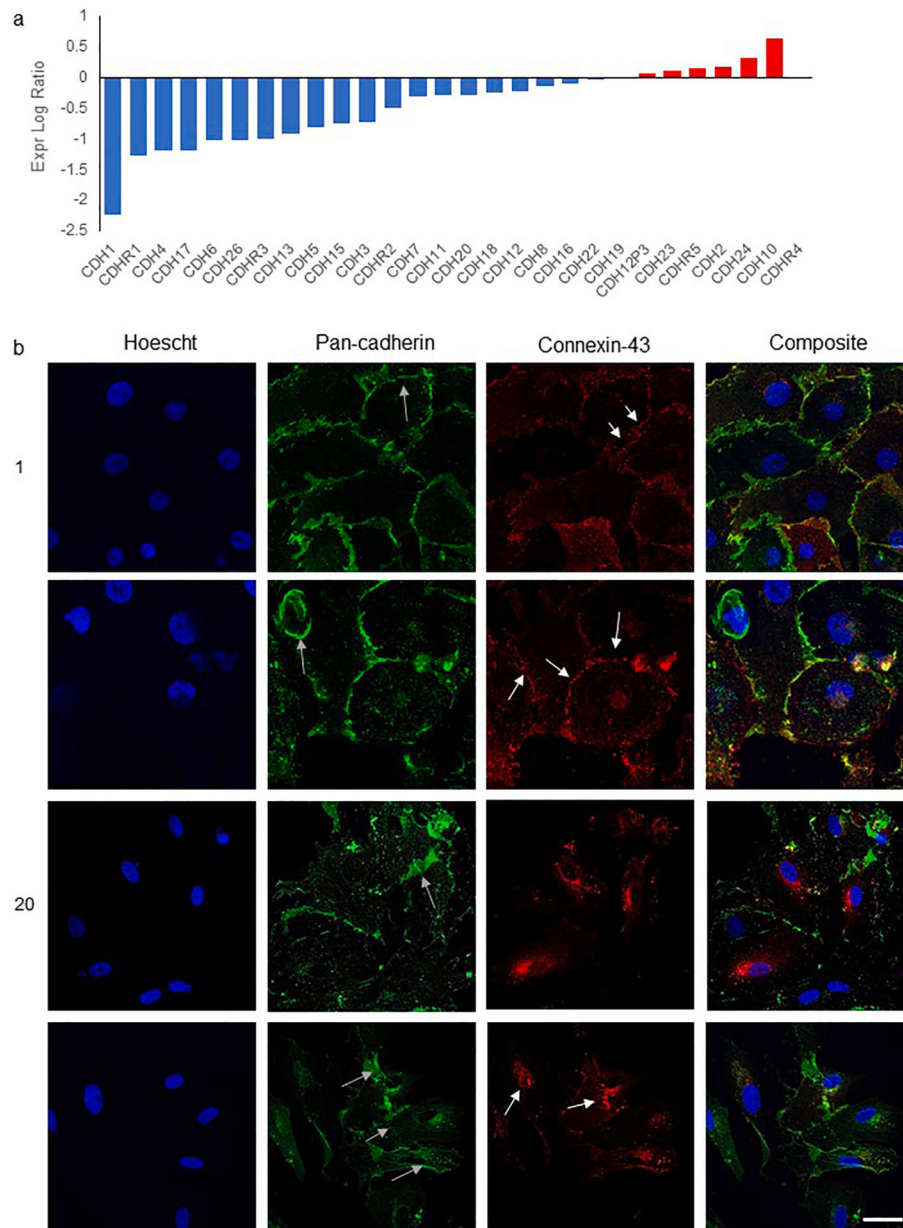
Fig. 6.
Dysregulation and changes in the localization of pan-cadherin and connexin-43. (a) Transcriptomics analysis showed that multiple cadherins were down-regulated after exposure to TNF-α. (b) Immunocytochemistry analysis of pan-cadherin marker and Connexin-43 using representative images from CM derived from SCVI 273.
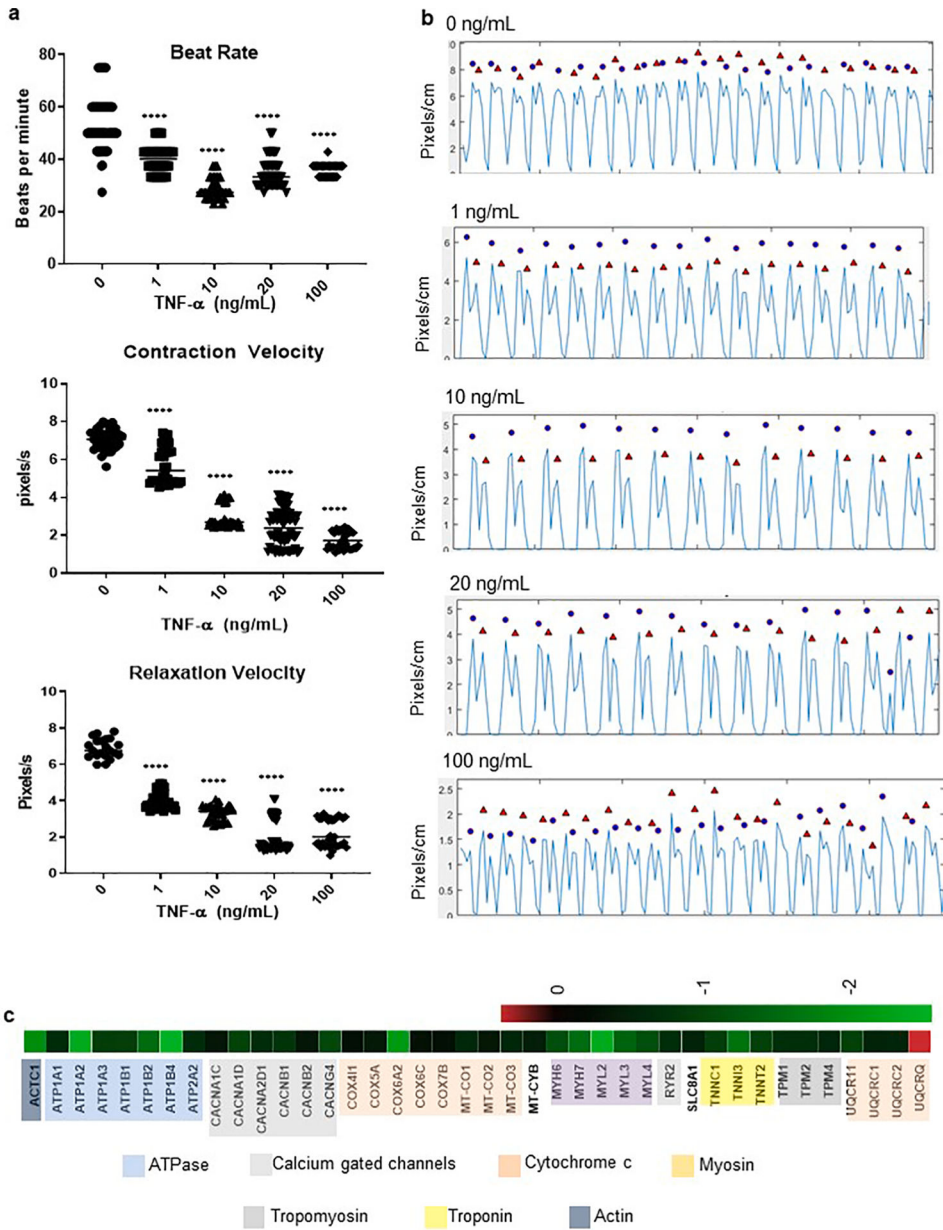
Fig. 7.
Contractility of hiPSCs-CMs decreased after TNF-α treatment. (a) Summary of hiPSC-CM contractility analysis (n = 30–70). (a) Representative traces of beating patterns of hiPSC-CMs. Ectopic and irregular beating is noted with higher concentrations of TNF-α (black arrows). (c) Transcriptomics analysis showing that expression of genes associated with aerobic respiration as well as contractile proteins were downregulated. Statistical analyses were performed by one-way ANOVA and post-hoc analysis was performed by Tukey's multiple comparison test *p < 0.05, **p < 0.01, *** p < 0.001, ****p < 0.0001.